Journal of
Data Acquisition and Processing

ISSN: 1004-9037
https://sjcjycl.cn/
DOI: 10.5281/zenodo.777660

A SIZABLE AND SUPERIOR GROUND TRUTH URBAN POINT CLOUD DATASET FOR AUTOMATED SEGMENTATION AND CLASSIFICATION IS PARIS-LILLE-3D.

Dr. Sunil Kumar Mishra
CSE Dept

Dr. Yogesh Bhomia
ECE Dept

Mr. Sudarshan Singh
CSE Dept
Accurate Institute Of Management & Technology, Greater Noida

Abstract

In this research, a new Urban Point Cloud Dataset obtained by Mobile Laser Scanning (MLS) for Automatic Segmentation and Classification is presented. We go over the steps involved in obtaining the dataset, from acquisition to labelling and post-processing. This dataset can be used to train pointwise classification algorithms, but it can also be used to train object recognition and segmentation algorithms because of the careful attention that has been paid to the divide between the various objects. About 2 km of MLS point cloud that were collected in two cities make up the dataset. The quantity of points and variety of classes lead us to believe that Deep-Learning techniques can be trained with it. Additionally, we display a few outcomes of our automated segmentation and categorization. The dataset is available at: http://caor-mines-paristech.fr/fr/paris-lille-3d-dataset/.

Keywords: Urban Point Cloud, Dataset, Classification, Segmentation, Mobile Laser Scanning

1 Introduction

As machine learning techniques for segmenting and classifying 3D point clouds advance, an increasing amount of data, both in terms of quantity and quality (number of points, number of classes, and segmentation quality), are required.

More datasets for image classification and segmentation, visual and LiDAR odometry or SLAM, vehicle and pedestrian detection in films, stereo vision, optical flow, etc., are constantly being added. Finding datasets with segmented and classed urban 3D point clouds is still challenging, though. The datasets listed in section Available Datasets are the only ones that are comparable. While each of them has pros and cons, we don't think any of them fully encapsulates the benefits of the dataset we make public.

We present our newly produced metropolitan dataset, Paris-Lille-3D, in the section "Our Dataset." The objects in this dataset are adequately segmented to allow for very fine segmentation learning. Our dataset can be found at the following address: http://caor-mines-paristech.fr/fr/paris-lille-3d-dataset/.

In section Results of automatic segmentation and classification, we give some results of automatic segmentation and classification on our dataset.

2 Available Datasets

Numerous datasets are used for training and benchmarking machine learning algorithms. The provided data allows for the training of methods that perform a given task, and the evaluation of performance on a test set allows evaluation of the quality of the results obtained and comparison of different methods according to various metrics.

Many different tasks can be learned, the most common being classification (for example, for an image, it is giving the class of the principal object visible). Another task may be to segment the data into its relevant parts (for the images it is grouping all the pixels that belong to the same object). There are multiple other tasks that can be learned, from image analysis to translation in natural language processing, for a survey see [FMH+15].

There is a bunch of existing datasets in many fields. Each dataset has different types of data, in type (image, sound, text, point clouds, graphs), quantity (from hundreds to billion of samples), quality, number of classes (from tens to thousands), and tasks to learn. Amongst the most famous are:

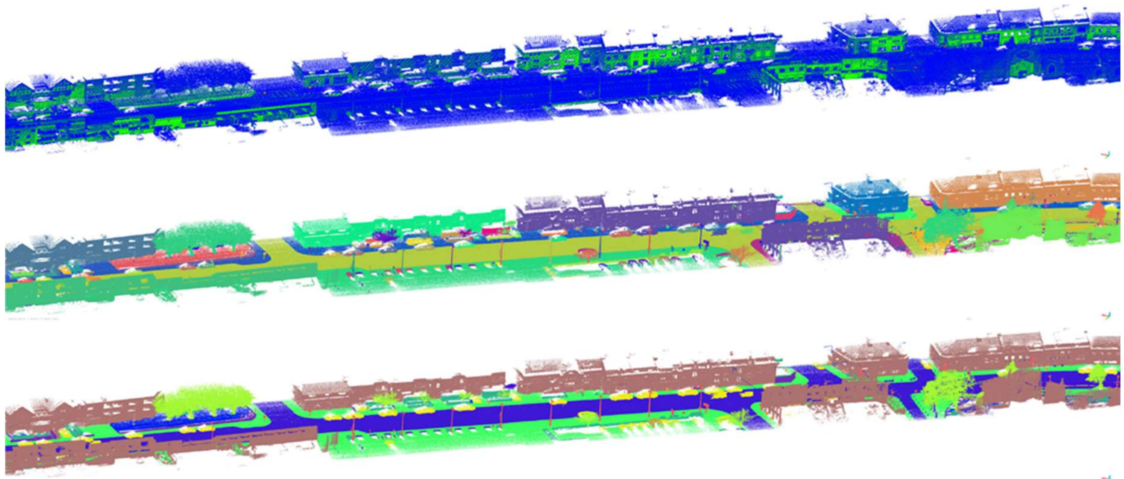

Figure 1: Part of our dataset. Top: reflectance from blue(0) to red(255), middle: object label (different color for each object), bottom: object class (different color for each class).

Name	Lidar type	Length	Number of points	Number of classes
Oakland	MLS mono-fiber	1510m	1.61M	44
Semantic3D	static LiDAR	–	1660M	8
Paris-rue-Madame	MLS multi-fiber	160m	20M	17
IQmulus	MLS mono-fiber	210m	12M	22
Paris-Lille-3D	MLS multi-fiber	1940m	143.1M	50

Table 1: Comparison of urban 3D point cloud datasets.

. image classification and segmentation datasets: ImageNet [DDS+09], MS COCO [LMB+14],
. stereovision dataset for depth map estimation: Middlebury Stereo Datasets [SHK+14],
. video dataset: Youtube-8M [AEHKL+16],
. odometry, stereovision, optical flow and 3D object detection dataset: KITTI [GLU12],

. SLAM dataset: Ford Campus Vision and Lidar Data Set [PME11],
. long-term localization datasets: the Oxford Robotcar Dataset [MPLN17] and the NCLT Dataset [CBUE16],
. urban street image segmentation dataset: The Cityscapes Dataset [COR+16].
Closer to our field of research are Airborne Laser Scanning (ALS) datasets as provided with the 3D Semantic Labeling Contest [NRS14].
The data we are interested in are urban 3D point clouds. There are mainly two methods that allow to acquire these data in quality sufficient for us:
. Mobile Laser Scanning (MLS), with a LiDAR mounted on a ground vehicle or a drone. To register the clouds, an accurate 6D-pose of the vehicle must be known.
. Terrestrial Laser Scanning (TLS) by static LiDAR, the LiDAR must be moved between each acquisition and clouds must be registered.
The ALS does not allow to obtain a sufficient density of points because of the distance and the angle of acquisition.
There are already some segmented and classified urban 3D point cloud datasets. However these datasets are very het- erogeneous and each has features that can be seen as defects. In the 4 next sub-sections, we make a comparison of the existing datasets and identify their strengths and weaknesses for automatic classification and segmentation. Table 1 presents a quantitative comparison of these datasets with ours.

2.1 Oakland 3-D Point Cloud Dataset [MBVH09]

This dataset was acquiered by a MLS system mounted with a side looking Sick monofiber LiDAR. Since it is a mono-fiber LiDAR, it has the disadvantage of hitting the objects from a single point of view, so there are many occlusions. In addition it is much less dense than other datasets because of the low acquisition rate of the LiDAR (see figure 2). In addition, this dataset contains 44 classes of which a large part (24) have less than 1000 labeled points. This is very low to be able to distinguish objects, especially when these points are distributed over several samples.

Figure 2: Example of cloud in Oakland dataset. Low density, few classes, big shadows behind trees (due to monofiber LiDAR).

2.2 Semantic3D [HWS16]

This dataset was acquired by static laser scanners. It is therefore much more precise and dense than a dataset acquired by MLS, but it has disadvantages inherent to static LiDARs (see figure 3):

. The density of points varies considerably depending on the distance to the sensor.

. There are occlusions due to the fact that sensors do not turn around the objects. Even by registering several clouds acquired from different viewpoints, there are still a lot of occlusions.

. The acquisition time is much more important than by MLS, which prevents to obtain very miscellaneous scenes.

Figure 3: Example of cloud in Semantic3D dataset (3 clouds registered). Occlusions, density depends on the distance to the LiDAR.

2.3 Paris-rue-Madame Database [SMGD14]

This dataset was acquired by an earlier version of our MLS system [GNA+06]. This dataset was segmented and annotated semi-automatically, first by a mathematical morphology method on elevation images [SMGD14] and then refined by hand. Some segmentation inaccuracies at the edges of objects remain (see figure 4), in particular the bottom of the objects is annotated as belonging to the ground. Moreover, the system as well as the point cloud processing pipeline have been greatly improved. We can now generate clouds much less noisy.

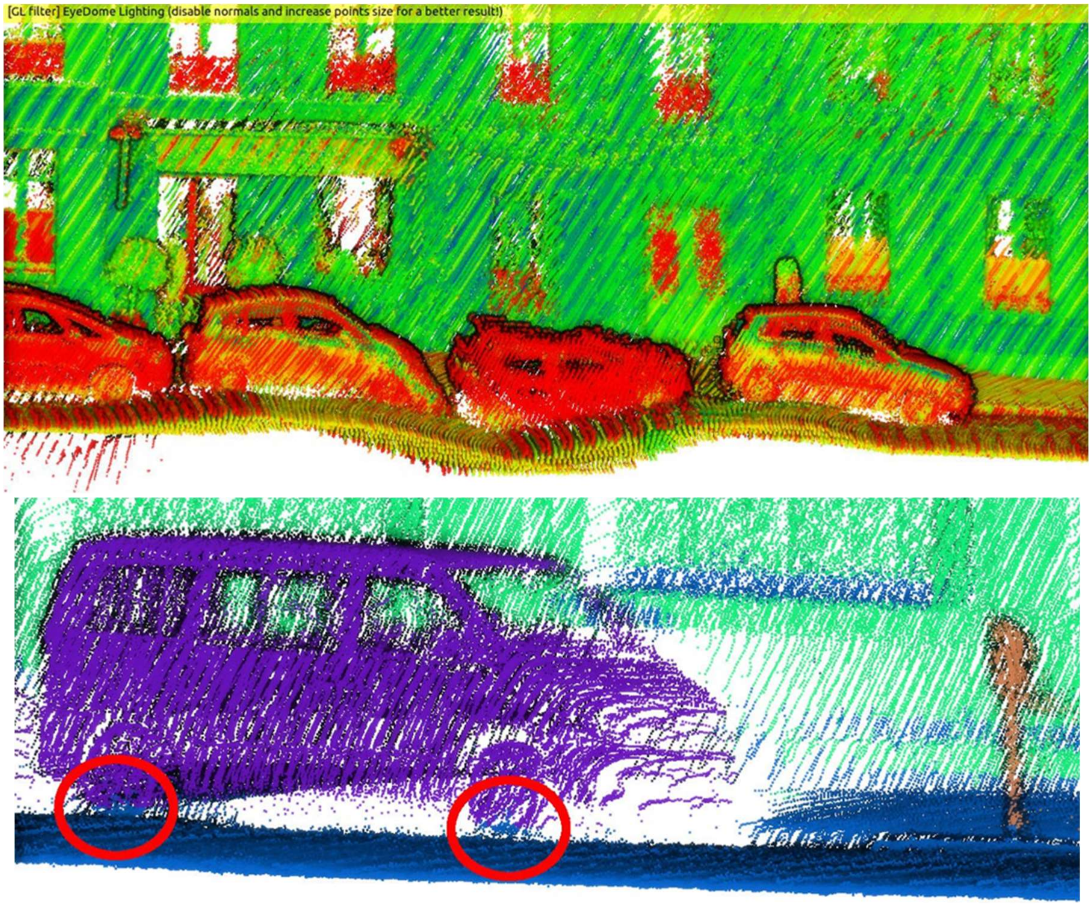

Figure 4: Example of cloud in Rue-Madame dataset. Ground truth mistakes: can be very noisy (top), parts of cars are seen as road (bottom).

2.4 IQmulus & TerraMobilita Contest [VBS+15]

This dataset was acquired by a MLS system mounted with a monofiber Riegl LMS-Q120i LiDAR. This LiDAR has the advantage of being more accurate than a multi-fiber LiDAR such as the Velodyne HDL-32E, but it is also more expensive. Moreover, since it is mono-fiber, it has the disadvantage of hitting the objects from a single point of view, so there are many occlusions.
For the annotation, the scan lines of the LiDAR were concatenated one above the other to form 2D images. The values of the pixels are the intensity of laser return.

This method has the advantage of being easy to put into production, which allowed the IGN to annotate a large dataset. However, inaccuracies in countouring annotation of 2D images generate badly classified points, the points around the occlu- sions are classified in the class of the object that creates the occlusion. (see figure 5).

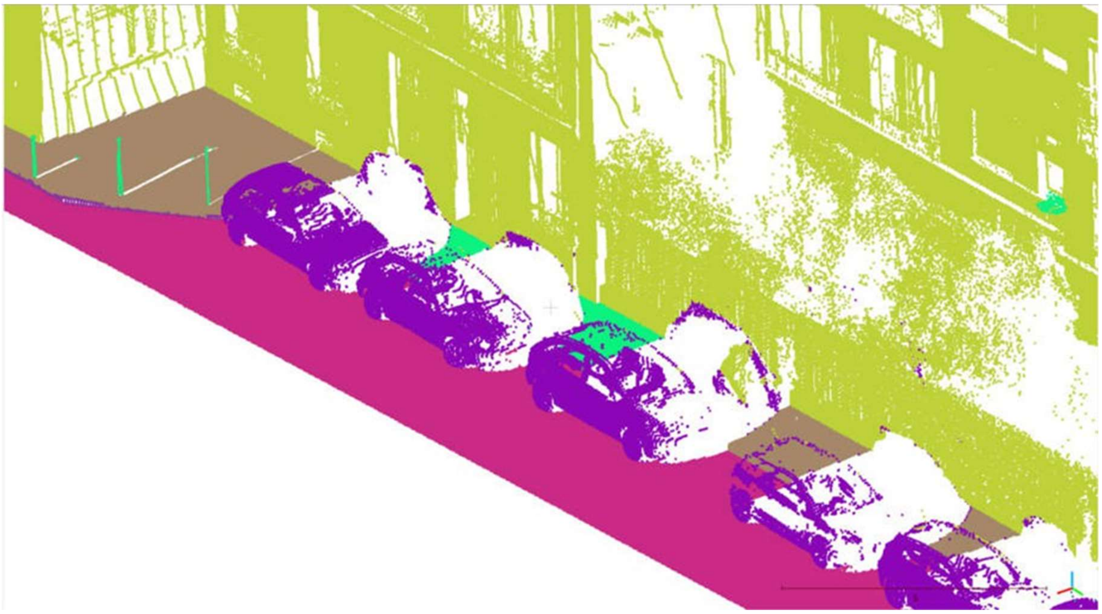

Figure 5: Example of cloud in iQmulus/TerraMobilita dataset. As a monofiber LiDAR is used, there are shadows behind objects. Moreover points of the wall behind cars are classified as car.

3 Our Dataset: Paris-Lille-3D

3.1 Acquisition

All point clouds used in our dataset were acquired with the MLS prototype of the center for robotics of Mines ParisTech: L3D2 [GNA+06] (as seen in figure 6). It is a Citroën Jumper equipped with a GPS (Novatel FlexPak 6), an IMU (Ixsea PHINS in LANDINS mode) and a Velodyne HDL-32E LiDAR mounted at the rear of the truck with an angle of 30 degrees between the axis of rotation and the horizontal.

Figure 6: MLS prototype: L3D2

For localization, we use a dual-phase L1/L2 RTK-GPS at 1Hz with a fixed base provided by the IGN RGP1 (Permanent GNSS Network). RGP bases are: SMNE for Paris dataset and LMCU for Lille dataset. The IMU sends data at 100Hz. Data from the LiDAR and IMU are synchronised thanks to PPS signal from the GPS.
In post-process, we retrieve data from RGP fixed base, and we generate the trajectory with the Inertial Explorer2 software. The method used is Tightly Coupled GPS-RTK/INS Kalman Smoothing EKF. We obtain a trajectory in WGS84 system at 100Hz, that we convert to Lambert RGF93.
Then, as each point has its own timestamp, we linearly interpolate the trajectory. Moreover we only keep points measured at a distance less than 20m in order to keep only areas of sufficiently high density. Finally we build clouds for which each point is characterized by a vector (x, y, z, xorigin, yorigin, zorigin, t, i), where i is the intensity of the LiDAR return.
We do not apply any method of SLAM, cloud registration or loop closure. All trajectories are built with Inertial Explorer.

3.2 Description of point clouds

The dataset consists of three parts, two parts in the agglomeration of Lille and one in Paris (see figure 7).

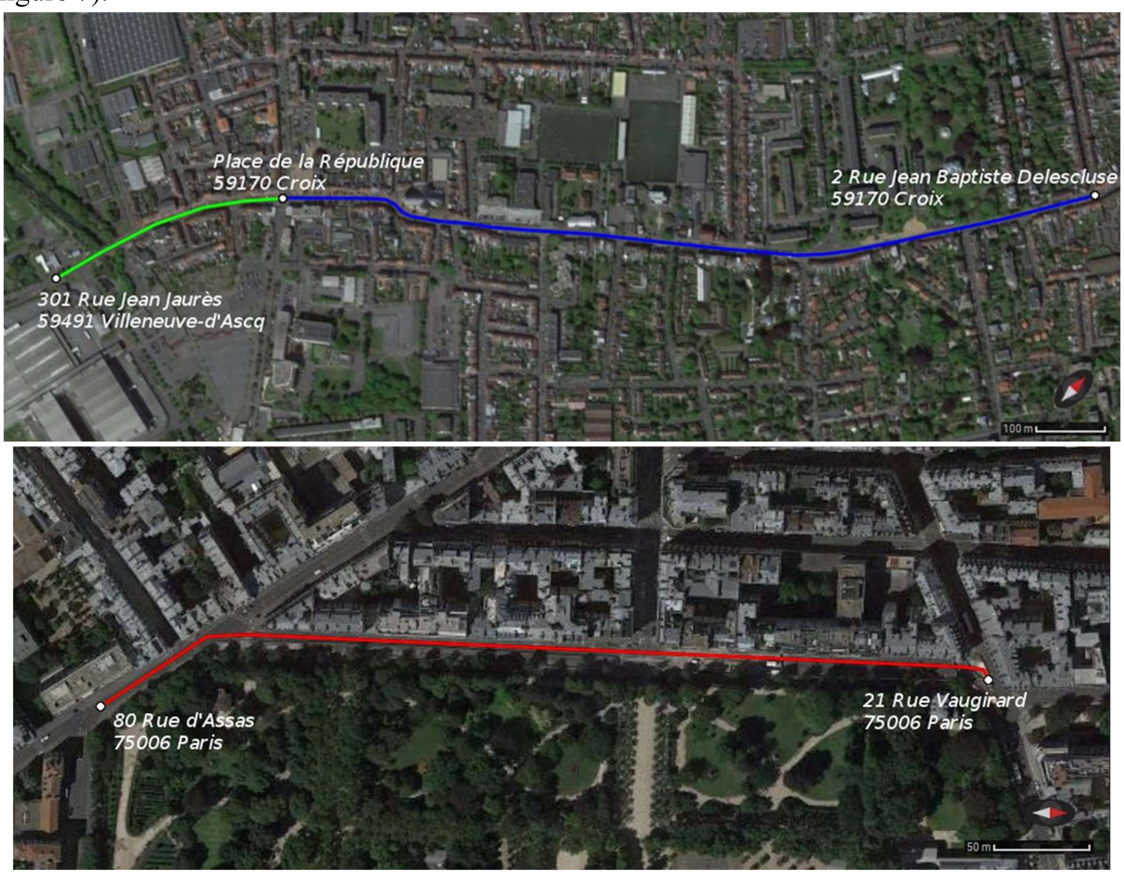

Figure 7: Trajectories of the experimental vehicle during acquisition. Top: the 2 trajectories in agglomeration of Lille are in green and blue. Bottom: the trajectory in Paris is in red. (Pictures from Google Maps)

For the sake of precision, an offset has been substracted in the plane (x,y) to all the points so that they hold in float (32 bits). Data are distributed as explained in table 2.

Section	Length	Number of points	RGF93 Offset
Lille1	1150m	71.3M	(711164.0m, 7064875.0m)
Lille2	340m	26.8M	(711164.0m, 7064875.0m)
Paris	450m	45.7M	(650976.0m, 6861466.0m)
Total	1940m	143.1M	–

Table 2: Description of the three parts of the dataset.

The clouds have high density with between 1000 and 2000 points per square meter on the ground, but there are some anisotropic patterns due to the multi-beam LiDAR sensor as seen in figure 8.

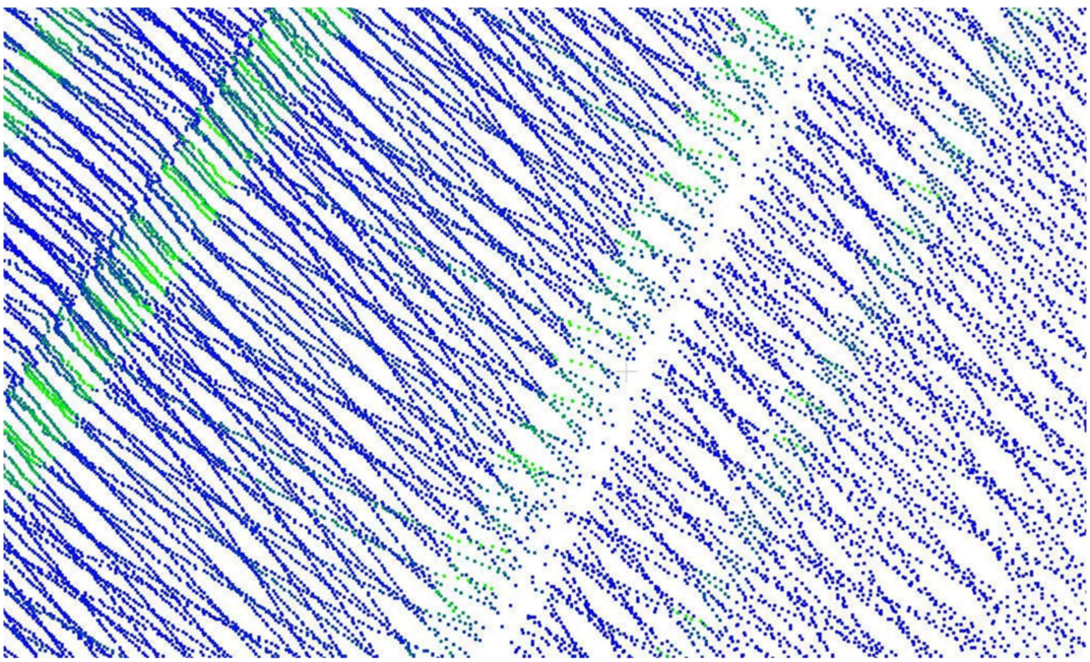

Figure 8: Anisotropic pattern on the ground (color of points is the reflectance)

3.3 Description of segmented and classified data

The clouds obtained were segmented and classified by hand using CloudCompare3 software. Some illustrations of the seg- mented and classified data are shown in figure 1.

We chose to re-use the class tree of iQmulus/Terramobilita benchmark, in which we only change a few classes and add classes relevant to our dataset. It can be found at url: http://data.ign.fr/benchmarks/UrbanAnalysis/download/ classes.xml For a distribution of number of points by classes, see table 3. Classes added:

. bicycle rack (id = 302021200)
. statue (id = 302021300)
. distribution box (id = 302040600)
. lighting console (id = 302040700)
. windmill (id = 302040800)

We also change the way vehicles are seen. More precisely, for each class of vehicle, we distinguish sub-classes depending on whether they are parked, stopped (on the road) or moving. And Velib terminal is changed to bicycle terminal (id = 302021100) which is more generic.
Except the few classes mentioned above, this class tree appears to be sufficiently complete for classes encountered in our dataset. The XML file describing this tree is named classes.xml and is provided with the dataset. We also provide three ASCII-files (.txt) containing annotations for particular samples. Each line of these files contains:
sample_id, class_id, class_name, annotation1, annotation2, ...
The most common annotations are:
. "several", for example when trees are interlaced and can not be delimited precisely by hand,
. "overturned", for trash cans laid on their side.

3http://www.danielgm.net/cc/

Class	Number of samples (of points)							
	Lille1		Lille2		Paris		Total	
unclassified	1	(54.88k)	1	(16.47k)	1	(60.79k)	3	(132.1k)
other	16	(70.15k)	11	(14.10k)	11	(30.82k)	38	(115.1k)
road	1	(34.80M)	1	(11.82M)	1	(19.68M)	3	(66.30M)
sidewalk	18	(8.566M)	8	(4.97M)	5	(4.6M)	31	(16.67M)
island	7	(458.8k)	0	(0)	9	(82.46k)	16	(541.2k)
vegetation	32	(562.2k)	22	(512.4k)	6	(157.1k)	60	(1.232M)
building	34	(18.2M)	8	(7.934M)	5	(9.431M)	47	(35.39M)
post	9	(13.51k)	0	(0)	0	(0)	9	(13.51k)
bollard	122	(34.80k)	64	(7.982k)	84	(28.33k)	270	(71.10k)
floor lamp	72	(232.9k)	13	(23.69k)	21	(113.2k)	106	(369.7k)
traffic light	14	(25.82k)	11	(27.41k)	16	(80.76k)	41	(133.10k)
traffic sign	82	(113.6k)	39	(69.89k)	17	(30.75k)	138	(214.3k)
signboard	20	(68.34k)	12	(43.14k)	3	(13.41k)	35	(124.9k)
mailbox	0	(0)	0	(0)	1	(4.739k)	1	(4.739k)
trash can	11	(14.72k)	6	(17.43k)	22	(30.35k)	39	(62.50k)
meter	0	(0)	0	(0)	2	(2.840k)	2	(2.840k)
bicycle terminal	10	(1.736k)	0	(0)	13	(6.451k)	23	(8.187k)
bicycle rack	8	(774)	0	(0)	14	(8.665k)	22	(9.439k)
statue	2	(4.158k)	0	(0)	0	(0)	2	(4.158k)
barrier	45	(83.94k)	5	(9.286k)	7	(56.10k)	57	(149.3k)
roasting	6	(831.0k)	1	(20.82k)	4	(1.677M)	11	(2.529M)
wire	34	(14.18k)	8	(9.325k)	0	(0)	42	(23.51k)
low wall	58	(840.2k)	2	(26.99k)	9	(951.4k)	69	(1.819M)
shelter	0	(0)	0	(0)	3	(83.45k)	3	(83.45k)
bench	5	(2.911k)	1	(364)	2	(1.391k)	8	(4.666k)
distribution box	19	(50.28k)	8	(14.89k)	3	(53.4k)	30	(118.2k)
lighting console	78	(7.251k)	60	(9.731k)	9	(4.393k)	147	(21.38k)
windmill	1	(10.17k)	0	(0)	0	(0)	1	(10.17k)
pedestrian	17	(24.81k)	7	(11.60k)	61	(150.2k)	85	(186.6k)
parked bicycle	15	(9.74k)	0	(0)	33	(81.67k)	48	(90.75k)
mobile scooter	0	(0)	0	(0)	1	(131)	1	(131)
parked scooter	0	(0)	0	(0)	31	(169.1k)	31	(169.1k)
mobile motorbike	0	(0)	0	(0)	1	(1.613k)	1	(1.613k)
parked motorbike	2	(2.428k)	0	(0)	4	(14.37k)	6	(16.79k)
mobile car	21	(175.0k)	4	(40.96k)	5	(66.35k)	30	(282.3k)
stopped car	0	(0)	1	(28.27k)	1	(9.375k)	2	(37.64k)
parked car	182	(2.266M)	47	(853.7k)	65	(1.610M)	294	(4.730M)
mobile van	3	(97.27k)	1	(41.6k)	0	(0)	4	(138.3k)
parked van	5	(84.75k)	5	(85.20k)	9	(357.6k)	19	(527.6k)
stopped truck	0	(0)	0	(0)	1	(235.7k)	1	(235.7k)
parked truck	2	(40.32k)	0	(0)	1	(53.44k)	3	(93.76k)
stopped bus	0	(0)	0	(0)	1	(78.41k)	1	(78.41k)
parked bus	1	(9.623k)	0	(0)	0	(0)	1	(9.623k)
table	0	(0)	0	(0)	2	(576)	2	(576)
chair	0	(0)	0	(0)	8	(4.842k)	8	(4.842k)
trash can	138	(148.8k)	80	(115.9k)	0	(0)	218	(264.7k)
waste	5	(2.307k)	0	(0)	0	(0)	5	(2.307k)
natural	149	(1.233M)	47	(396.9k)	36	(1.610M)	232	(3.240M)
tree	72	(2.310M)	23	(565.10k)	101	(4.755M)	196	(7.631M)
potted plant	32	(72.80k)	5	(26.96k)	0	(0)	37	(99.76k)
Total	1349	(71.36M)	501	(26.84M)	629	(45.80M)	2479	(143.10M)

Table 3: Number of samples/points for each class (k for thousand and M for million). Trash cans appear twice, the first time is for only fixed trash can.

3.4 Description of files

Each part of the dataset is in a separate PLY-file, a summary of each file can be found in table 4. Each point of PLY-files has 10 attributes:
. x, y, z (float) : the position of the point,

. x_origin, y_origin, z_origin (float) : the position of the LiDAR,
. GPS_time (double) : the moment when the point was acquired,
. reflectance (uint8) : the intensity of laser return,
. label (uint32) : the label of the object to which the point belongs,
. class (uint32) : the class of the object to which the point belongs.

Section	Length	Number of points	Number of objects	Number of classes
Lille1	1150m	71.3M	1349	39
Lille2	340m	26.8M	501	29
Paris	450m	45.7M	629	41
Total	1940m	143.1M	2479	50

Table 4: Overview of our dataset.

4 Results of automatic segmentation and classification

In this section, we evaluate an automatic segmentation and classification method on our dataset. There are many approaches to achieve this task, most of them look like one of the following pipelines:
. classify each point for example by computing local features (hand-made [WJHM15] or by Deep-Learning methods [?]), then group them into objects for example by CRF methods (see [?]).
. segment the cloud into segments, for example by mathematical morphology (see [SM14]) or supervoxel (see [ACT13]), then classify each segment (by hand-made global descriptors [JH99, VSS12] or by deep-learning [MS15, QSMG16]).
The method used here [RDG16] belongs to the first category. The detailed processing pipeline is:
. extraction of the ground by region growing on an elevation map,
. segmentation of objects by connectivity of the remaining point cloud,
. computation of descriptors on each object (some simple geometric descriptors inspired by [SM14] and some 3D de- scriptor of the literature as CVFH [RBTH10], GRSD [MPB+10] and ESF [OFCD01]),
. classification of the objects with a Random Forest.

4.1 Improvements of [RDG16]

Two improvements are proposed to increase the robustness of this method: first on the segmentation by new extraction of the ground (using better seed for the region growing), then on the classification with new descriptors (to take the context of objects into account).

4.1.1 Ground Extraction

In [RDG16], the seed for region growing is found by computing a histogram in z on the whole cloud, which is not robust in case the road is sloping. As we know the exact position of the LiDAR sensor with respect to the ground (2.71m above ground), we can extract the points that are just below the sensor in a cylinder parameterized by:

$$\sqrt{(x-x_{origin})^2 + (y-y_{origin})^2} \leq 1 \tag{1}$$

$$|z_{origin} - z - 2.71| \leq 0.3 \tag{2}$$

Points lying in this cylinder are then taken as seeds for the region growing.

4.1.2 Features for Classification

It was observed that some objects (such as cars) were detected way above the ground. We propose to solve this problem by adding a contextual descriptor which gives the altitude of the object with respect to the ground detected in the previous step.

In a first step we calculate an image of elevation of the ground, for example with a resolution 10cm × 10cm. Then empty

pixels are filled with elevation of the closest non-empty pixel. And the image is smoothed to avoid segmentation artefacts (for example where the ground meets the foot of the buildings).

Then for each object, the barycenter is projected onto this elevation image of the ground, which gives us the elevation of the ground under this object: zground. If zmin is the minimum elevation of the object, the descriptor added is: zmin −zground.

4.2 Evaluation: Segmentation

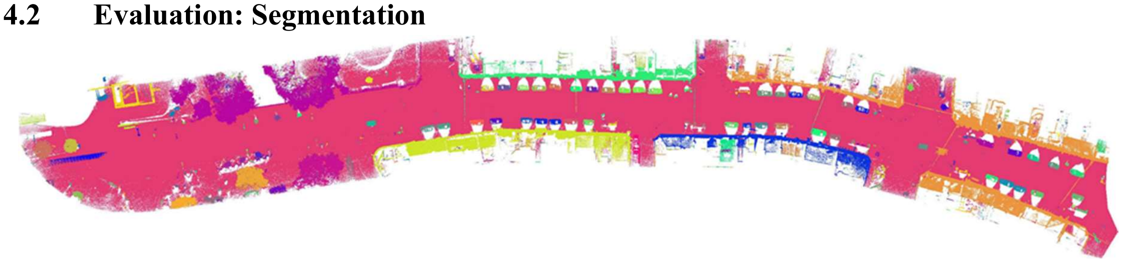

Figure 9: Exemple of cloud segmented by our method (each object has a different color).

Our segmentation method is very basic, indeed it makes very strong a priori on the way to distinguish objects from each other. Two objects are different if they are in different connected component of the point cloud from which the ground has been removed. This explains some problems (see figure 10) like two cars too close one from another segmented as a single object, or buildings just linked by a cable.

Our segmentation method is very basic, indeed it makes very strong a priori on the way to distinguish objects from each other. Two objects are different if they are in different connected components of the point cloud from which the ground has been removed. This explains some problems (see figure 10) like two cars too close one from another segmented as a single object, or buildings just linked by a cable.

To evaluate detection of objects, we use the same metric as used in iQmulus/TerraMobilita contest [VBS+15].
For an object of the ground truth (represented by the subset SGT) and an object resulting from our segmentation method (SSR), we estimate that they match if the following conditions are respected:

$$\frac{|S^{GT}|}{|S^{GT} \cup S^{SR}|} > m \quad \text{and} \quad \frac{|S^{SR}|}{|S^{GT} \cup S^{SR}|} > m$$

Then detection precision and recall are computed by the following formulas:

$$precision(m) = \frac{\text{number of detected objects matched}}{\text{number of detected objects}}$$

$$recall(m) = \frac{\text{number of detected objects matched}}{\text{number of ground truth objects}}$$

$$F1(m) = \frac{2\, precision(m) \cdot recall(m)}{precision(m) + recall(m)}$$

We evaluate our results with m = 0.5 which is the minimal value that ensures that a Ground Truth object matches at most one object segmented by our method (see table 5).

Dataset	Precision	Recall	F1
Lille1	70.24%	38.55%	49.78%
Lille2	59.09%	31.71%	41.27%
Paris	54.24%	28.46%	37.33%

Table 5: Precision and Recall of object detection for $m = 0.5$.

It is believed that methods that learn segmentation will yield much better results.

4.3 Evaluation: Classification

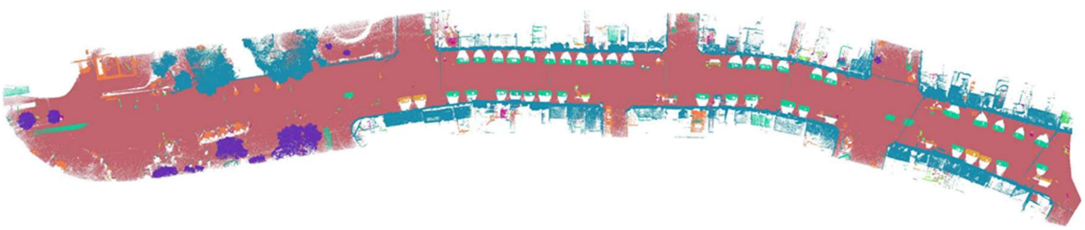

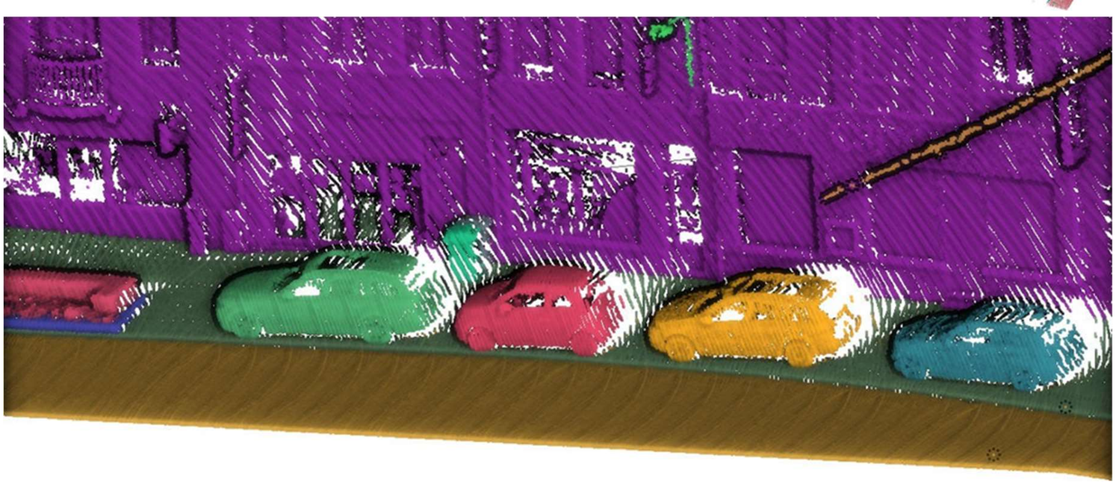

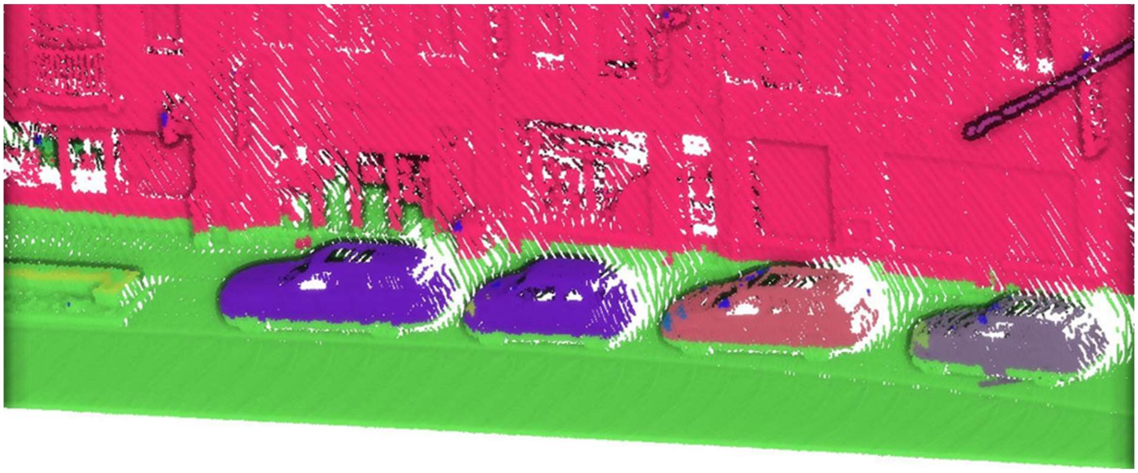

Figure 10: Comparison between clouds segmented automatically by our method (bottom) and by hand (top). Each object has a different color. Two cars too close one from another are segmented as a single object. The bottom part of each object is segmented as part of the ground. A trash can placed against the facade is seen as a part of the facade.

Figure 11: Example of cloud classified by our method (each class has a different color).
In this section we only evaluate the classification method assuming good segmentation. To do this, we take the set of objects of the dataset that are randomly divided into a training set (80%) and a test set (20%). We use only a few coarser classes than described in table 3 to evaluate our classification algorithm, see table 6 for a distribution of samples per class. In addition, we add a coarse_classes.xml file to the dataset that adds a coarse field to each class.

Class	Number of samples (of points)							
	Lille1		Lille2		Paris		Total	
buildings	34	(18.2M)	8	(7.934M)	5	(9.431M)	47	(35.39M)
poles	177	(385.9k)	63	(120.10k)	54	(224.7k)	294	(731.5k)
bollards	122	(34.80k)	64	(7.982k)	84	(28.33k)	270	(71.10k)
trash cans	149	(163.5k)	86	(133.3k)	22	(30.35k)	257	(327.2k)
barriers	109	(1.755M)	8	(57.9k)	20	(2.685M)	137	(4.497M)
pedestrians	17	(24.81k)	7	(11.60k)	61	(150.2k)	85	(186.6k)
cars	211	(2.623M)	58	(1.49M)	80	(2.43M)	349	(5.715M)
natural	221	(3.543M)	70	(962.8k)	137	(6.365M)	428	(10.87M)
Total	1040	(26.55M)	364	(10.28M)	463	(20.96M)	1867	(57.79M)

Table 6: Number of samples/points for each coarse class used for classification evaluation.
Even with these coarse classes, there are a few samples in some of them. Then precision and recall numbers in table 7 should be taken with caution. Metrics used to evaluate performance are the following:

$$\begin{aligned} P &= \frac{TP}{TP+FP} \\ R &= \frac{TP}{TP+FN} \\ F1 &= \frac{2TP}{2TP+FP+FN} \\ MCC &= \frac{TP\cdot TN - FP\cdot FN}{\sqrt{(TP+FP)(TP+FN)(TN+FP)(TN+FN)}} \end{aligned} \tag{3}$$

Where P, R, F1 and MCC represent respectively Precision, Recall, F1-score and Matthews correlation coefficient. And TP, TN, FP and FN are respectively the number of True-Positives, True-Negatives, False-Positives and False-Negatives.

Moreover, it can be noted that the best results are obtained with the combination of descriptors: Geometric and GRSD, which are the descriptors composed of the least number of variables. This can be explained by the few samples of the dataset and therefore adding a large number of features does not provide more relevant information. Then this dataset is more appropriate for the evaluation of per-point classification methods.

Descriptors	OOB	Accuracy	Precision	Recall	F1	MCC
Geom	89.22%	**98.08**%	89.48%	**85.13**%	**87.23**%	**85.62**%
CVFH	70.32%	94.68%	67.23%	60.82%	63.85%	60.14%
GRSD	70.02%	94.58%	64.42%	61.39%	62.82%	58.78%
ESF	74.98%	95.47%	70.87%	66.99%	68.85%	65.71%
Geom+CVFH	81.94%	96.76%	79.90%	74.76%	77.21%	74.65%
Geom+GRSD	**89.37**%	98.07%	**90.33**%	83.73%	86.89%	84.78%
Geom+ESF	82.45%	96.81%	81.25%	77.80%	79.46%	77.30%
CVFH+GRSD	75.98%	95.67%	74.62%	68.93%	71.62%	68.33%
CVFH+ESF	76.59%	95.76%	74.56%	68.81%	71.54%	68.38%
GRSD+ESF	79.13%	96.19%	77.42%	73.98%	75.63%	73.02%
Geom+CVFH+GRSD	83.00%	96.98%	81.54%	76.03%	78.64%	76.10%
Geom+CVFH+ESF	82.23%	96.76%	81.75%	76.89%	79.22%	76.88%
Geom+GRSD+ESF	83.90%	97.05%	82.26%	79.65%	80.91%	78.90%
CVFH+GRSD+ESF	79.25%	96.27%	79.04%	74.04%	76.43%	73.75%
Geom+CVFH+GRSD+ESF	83.41%	97.00%	82.91%	79.07%	80.92%	78.78%

Table 7: Classification performance for each combination of descriptors, these metrics are averaged over all classes (the OOB score is given by Random-Forest during training).

It can be concluded that it is not necessary to calculate all the descriptors to obtain the best classification results. It is possible to gain in computation time by calculating only the geometric descriptors and GRSD (see table 8 for precise gains).

And for applications where time is critical, we can even calculate only the geometric descriptors (which also avoids having to calculate the normals).

Descriptors	Proportion	Mean Time per object (ms)
Geom	3.22%	0.9
CVFH	44.92%	11.9
GRSD	12.04%	3.2
ESF	39.82%	10.6
Total	100%	26.6
Normals		47.9

Table 8: Mean computational time for calculating descriptors on segmented objects. Time to compute normal vectors is added for comparison.

5 Conclusion

We presented a dataset of urban 3D point cloud for automatic segmentation and classification. This dataset contains 140 million points on 2km in two different cities. The objects were segmented by hand and a class was associated with each one among 50 classes.

We hope that this dataset will help to train and evaluate methods as deep-learning, which are very demanding in terms of quantity of points.

In addition, we have tested a first method of segmentation and automatic classification from [RDG16] to which we have made some improvements for robustness.

References

[ACT13] Ahmad Kamal Aijazi, Paul Checchin, and Laurent Trassoudaine. Segmentation based classification of 3d urban point clouds: A super-voxel based approach with evaluation. Remote Sensing, 5(4):1624–1650, 2013.

[AEHKL+16] Sami Abu-El-Haija, Nisarg Kothari, Joonseok Lee, Paul Natsev, George Toderici, Balakrishnan Varadarajan, and Sudheendra Vijayanarasimhan. Youtube-8m: A large-scale video classification benchmark. arXiv preprint arXiv:1609.08675, 2016.

[CBUE16] Nicholas Carlevaris-Bianco, Arash K Ushani, and Ryan M Eustice. University of michigan north campus long-term vision and lidar dataset. The International Journal of Robotics Research, 35(9):1023–1035, 2016.

[COR+16] Marius Cordts, Mohamed Omran, Sebastian Ramos, Timo Rehfeld, Markus Enzweiler, Rodrigo Benenson, Uwe Franke, Stefan Roth, and Bernt Schiele. The cityscapes dataset for semantic urban scene understanding. In Proceedings of the IEEE Conference on Computer Vision and Pattern Recognition, pages 3213–3223, 2016.

[DDS+09] Jia Deng, Wei Dong, Richard Socher, Li-Jia Li, Kai Li, and Li Fei-Fei. Imagenet: A large-scale hierarchical image database. In Computer Vision and Pattern Recognition, 2009. CVPR 2009. IEEE Conference on, pages 248–255. IEEE, 2009.

[FMH+15] Francis Ferraro, Nasrin Mostafazadeh, Ting-Hao Huang, Lucy Vanderwende, Jacob Devlin, Michel Gal- ley, and Margaret Mitchell. A survey of current datasets for vision and language research. arXiv preprint arXiv:1506.06833, 2015.

[GLU12] Andreas Geiger, Philip Lenz, and Raquel Urtasun. Are we ready for autonomous driving? the kitti vision benchmark suite. In Conference on Computer Vision and Pattern Recognition (CVPR), 2012.

[GNA+06] F Goulette, F Nashashibi, I Abuhadrous, S Ammoun, and C Laurgeau. An integrated on-board laser range sensing system for on-the-way city and road modelling. The International Archives of the Photogrammetry, Remote Sensing and Spatial Information Sciences, 34(Part A), 2006.

[HWS16] Timo Hackel, Jan D Wegner, and Konrad Schindler. Fast semantic segmentation of 3d point clouds with strongly varying density. ISPRS Annals of the Photogrammetry, Remote Sensing and Spatial Information Sciences, Prague, Czech Republic, 3:177–184, 2016.

[JH99] Andrew E Johnson and Martial Hebert. Using spin images for efficient object recognition in cluttered 3d scenes. Pattern Analysis and Machine Intelligence, IEEE Transactions on, 21(5):433–449, 1999.

[LMB+14] Tsung-Yi Lin, Michael Maire, Serge Belongie, James Hays, Pietro Perona, Deva Ramanan, Piotr Dollár, and C Lawrence Zitnick. Microsoft coco: Common objects in context. In European Conference on Computer Vision, pages 740–755. Springer, 2014.

[MBVH09] Delfina Munoz, J Andrew Bagnell, Nicolas Vandapel, and Martial Hebert. Contextual classification with functional max-margin markov networks. In Computer Vision and Pattern Recognition, 2009. CVPR 2009. IEEE Conference on, pages 975–982. IEEE, 2009.

[MPB+10] Zoltan-Csaba Marton, Dejan Pangercic, Nico Blodow, Jonathan Kleinehellefort, and Michael Beetz. General 3d modelling of novel objects from a single view. In Intelligent Robots and Systems (IROS), 2010 IEEE/RSJ International Conference on, pages 3700–3705. IEEE, 2010.

[MPLN17] Will Maddern, Geoff Pascoe, Chris Linegar, and Paul Newman. 1 Year, 1000km: The Oxford RobotCar Dataset. The International Journal of Robotics Research (IJRR), 36(1):3–15, 2017.

[MS15] Daniel Maturana and Sebastian Scherer. Voxnet: A 3d convolutional neural network for real-time object recognition. In Intelligent Robots and Systems (IROS), 2015 IEEE/RSJ International Conference on, pages 922–928. IEEE, 2015.

[NRS14] Joachim Niemeyer, Franz Rottensteiner, and Uwe Soergel. Contextual classification of lidar data and building object detection in urban areas. ISPRS journal of photogrammetry and remote sensing, 87:152–165, 2014.

[OFCD01] Robert Osada, Thomas Funkhouser, Bernard Chazelle, and David Dobkin. Matching 3d models with shape distributions. In Shape Modeling and Applications, SMI 2001 International Conference on., pages 154–166. IEEE, 2001.

[PME11] Gaurav Pandey, James R McBride, and Ryan M Eustice. Ford campus vision and lidar data set. The Interna- tional Journal of Robotics Research, 30(13):1543–1552, 2011.

[QSMG16] Charles R Qi, Hao Su, Kaichun Mo, and Leonidas J Guibas. Pointnet: Deep learning on point sets for 3d classification and segmentation. arXiv preprint arXiv:1612.00593, 2016.

[RBTH10] Radu Bogdan Rusu, Gary Bradski, Romain Thibaux, and John Hsu. Fast 3d recognition and pose using the viewpoint feature histogram. In Intelligent Robots and Systems (IROS), 2010 IEEE/RSJ International Conference on, pages 2155–2162. IEEE, 2010.

[RDG16] Xavier Roynard, Jean-Emmanuel Deschaud, and Francois Goulette. Fast and robust segmentation and classi- fication for change detection in urban point clouds. In ISPRS 2016-XXIII ISPRS Congress, 2016.

[SHK+14] Daniel Scharstein, Heiko Hirschmüller, York Kitajima, Greg Krathwohl, Nera Nešic´, Xi Wang, and Porter Westling. High-resolution stereo datasets with subpixel-accurate ground truth. In German Conference on Pattern Recognition, pages 31–42. Springer, 2014.

[SM14] Andrés Serna and Beatriz Marcotegui. Detection, segmentation and classification of 3d urban objects using mathematical morphology and supervised learning. ISPRS Journal of Photogrammetry and Remote Sensing, 93:243–255, 2014.

[SMGD14] Andrés Serna, Beatriz Marcotegui, François Goulette, and Jean-Emmanuel Deschaud. Paris-rue-madame database: a 3d mobile laser scanner dataset for benchmarking urban detection, segmentation and classifi- cation methods. In 4th International Conference on Pattern Recognition, Applications and Methods ICPRAM 2014, 2014.

[VBS+15] Bruno Vallet, Mathieu Brédif, Andrés Serna, Beatriz Marcotegui, and Nicolas Paparoditis. Terramo- bilita/iqmulus urban point cloud analysis benchmark. Computers & Graphics, 49:126–133, 2015.
[VSS12] Alexander Velizhev, Roman Shapovalov, and Konrad Schindler. Implicit shape models for object detection in 3d point clouds. In International Society of Photogrammetry and Remote Sensing Congress, volume 2, 2012.
[WJHM15] Martin Weinmann, Boris Jutzi, Stefan Hinz, and Clément Mallet. Semantic point cloud interpretation based on optimal neighborhoods, relevant features and efficient classifiers. ISPRS Journal of Photogrammetry and Remote Sensing, 105:286–304, 2015.